Microstructure changes induced by capillary condensation in catalyst layers of PEM fuel cells

Ma, Liang; Liu, Zhong-Sheng; Huang, Cheng; Chen, Su-Huan; Meng, Guang-Wei

Publisher's version / Version de l'éditeur:
https://doi.org/10.1016/j.ijhydene.2010.08.072
International Journal of Hydrogen Energy, 35, 22, pp. 12182-12190, 2010-09-20

Available at www.sciencedirect.com

ScienceDirect

journal homepage: www.elsevier.com/locate/he

Microstructure changes induced by capillary condensation in catalyst layers of PEM fuel cells

Liang Ma [a,b], Zhong-Sheng Liu [a,*], Cheng Huang [a], Su-Huan Chen [b], Guang-Wei Meng [b]

[a] Institute for Fuel Cell Innovation, National Research Council Canada, 4250 Wesbrook Mall, Vancouver, BC, Canada V6T 1W5
[b] Department of Mechanics, Nanling Campus, Jilin University, Changchun, 130025, PR China

ARTICLE INFO

Article history:
Received 6 July 2010
Received in revised form
14 August 2010
Accepted 18 August 2010
Available online 20 September 2010

Keywords:
PEM fuel cell
Catalyst layer
Microstructure change
Capillary condensation
Pt/C particles

ABSTRACT

This paper proposes a hypothesis for explaining Pt/C particles' coarsening inside the catalyst layers of a PEM fuel cell. The hypothesis includes the two parts: (1) due to capillary condensation a water-bridge could be formed between two neighboring nano-scale Pt/C particles at relative humidity under 100% when the surfaces of the Pt/C particles are hydrophilic; (2) the capillary force of the water-bridge tends to pull together the Pt/C particles. The relation is derived in this paper between the capillary force and the factors including the diameter of Pt/C particles, relative humidity, temperature, distance between the two neighboring Pt/C particles and water contact angle. A parametric study is performed showing some details about water-bridge formation. Finally, the stress level induced by the capillary force inside the Nafion thin-film connecting with the Pt/C particles is calculated. The result shows that the capillary force could be large enough to break apart the Nafion thin-film, facilitating the movement of Pt/C particles towards each other.

1. Introduction

Proton exchange membrane (PEM) fuel cells are electrochemical devices oxidizing hydrogen and generating electricity with high efficiency and zero green house gas emissions on site. Over the past two decades PEM fuel cells have been being developed for powering hydrogen fuel cell cars, which are currently available in demonstration models and are not yet ready for general public use. In order to commercialize hydrogen fuel cell cars, the lifetime and the cost of PEM fuel cells have to be tremendously improved. The minimum requirement on the lifetime of PEM fuel cells for automotive applications is 5000 h, 1.5 times higher than the actual lifetime 2000 h of the state-of-art PEM fuel cells under automotive (dynamic) operating conditions. However, the lifetime has already reached up to 15,000 h under stationary operating conditions [1,2]. The huge gap in terms of lifetime between dynamic operating conditions and stationary operating conditions is an interesting phenomenon, but there is little literature available about the failure mechanisms under dynamic operating conditions.

References [1–10] addressed different failure modes of PEM fuel cells. References [3–5] compared fresh catalyst layers with aged ones in terms of microstructure evolutions using transmission electron microscopy (TEM) and scanning electron microscopy (SEM). The TEM and SEM images show that the microstructure in catalyst layers goes through significant changes, suggesting that the microstructure change leads to performance degradation. The different microstructure changes that have been observed include: cracking, delamination, carbon corrosion, dissolution of the electrolyte, catalyst particle migration, catalyst ripening, carbon coarsening,

* *Corresponding author*. Tel.: +1 604 221 3068; fax: +1 604 221 3001.
E-mail address: Zhong-Sheng.Liu@nrc-cnrc.gc.ca (Z.-S. Liu).
0360-3199/$ – see front matter
doi:10.1016/j.ijhydene.2010.08.072

and catalyst-layer thinning. Basically there are two types of typical failure models in catalyst layers of PEM fuel cells: chemical degradation of the ionic conducting parts or mechanical failure. References [6,7] suggested that mechanical damage plays an important part in catalyst layers. Mechanical analysis at the MEA level has been performed by reference [8], which concludes that critical residual stresses accumulate and lead to mechanical fatigue in MEA after hydrothermal cycles. However the evolution in the microstructures of catalyst layers is still unclear.

Over the past several years, we have been putting efforts to understand the mechanisms of microstructure changes, especially, under dynamic operating conditions. In references [9,10] we proposed a mechanics model to explain the phenomenon of macro-scale delamination and cracks induced by thermal expansion and swelling. In this work, we focus on a different mechanism of microstructure changes of catalyst layers. Capillary condensation is of importance in porous materials [11–13] such as the catalyst layers of PEM fuel cells. Here we try to suggest a hypothesis about how a water-bridge, formed by water-vapor condensation between or among adjacent Pt/C particles, drives the displacements of Pt/C particles and eventually causes cracking, delamination and Pt/C coarsening.

In Section 2, we propose the hypothesis and its background. In Section 3, we try to relate the capillary force of a water-bridge inside a pair of identical sphere Pt/C solid particles, with the parameters such as relative humidity and temperature. This is done based on the Kelvin equation and the toroidal approximation theory. Then we present the results of the parametric studies in Section 4, showing how the capillary force changes with different parameters. Section 5 discusses the mechanical properties of the microstructures in the catalyst layers. In Section 6, we establish a mechanical model of a simplified microstructure that contains two Pt/C particles linked with Nafion thin-film, then apply the capillary force obtained in Section 4 to one of the Pt/C particles and calculate the stress inside the Nafion thin-film by finite element method (FEM) [14]. The calculation results indicate that the stress level is in the same order as the strength limit of Nafion material.

2. Hypothesis description

The space between adjacent Pt/C particles in a catalyst layer is usually in the order of several nanometers, which can be seen from TEM/SEM images of catalyst layers. In such a confined tiny space with hydrophilic surfaces, as shown in Fig. 1, liquid water can be formed through capillary condensation [11], especially, in cathode catalyst layers where water is produced from oxygen reduction reaction ($O_2 + 4H^+ + 4e^- = 2H_2O$). This phenomenon can be explained by the Kelvin Equation. A concave meniscus at liquid-vapor interface results in tensile stress inside the water-bridge, which tends to pull the Pt/C particles in contact with the water-bridge. When the Pt/C particles are restrained by a Nafion thin-film, which is connected with the other part of the catalyst layer, a certain level of stress inside the Nafion thin-film will be developed. When PEM fuel cells work under dynamic loads, relative humidity and temperature inside catalyst layers fluctuate and the size of water-bridges fluctuates accordingly. Thus the Pt/C particles in contact with the water-bridge are subject to a dynamic (periodic) capillary force, which will cause dynamic (periodic) stress inside the Nafion thin-film. Since dynamic stress accelerates materials failure in the form of micro-scale fracture, crack propagation and delamination. We tend to believe that the capillary force in the water-bridge can pull together the Pt/C particles in contact with the water-bridge through deforming or breaking the Nafion thin-film. In this way, the Pt/C particles will tend to adhere together forming large agglomerates. With a large agglomerate, the active electrochemical surface area of Pt catalysts drops. Moreover, oxygen diffusion through a large agglomerate becomes more difficult than through a small agglomerate, especially, when Knudsen diffusion [15] becomes dominant because of the small pore size (several nanometers) and the condensed liquid water fills smaller hydrophilic pores causing more difficulties for oxygen to diffuse into reaction sites. The combination of reduced active surface area and poor gas diffusion explains why agglomerate coarsening causes performance degradation. Although this microstructure evolution-process, as stated above, has not been physically observed and thus should be considered as a hypothesis, the following detailed analysis provides a certain level of confidence in this hypothesis. Note that short-range intermolecular forces (a solid particle to its adjacent solid particle) can become significant within the range of several nanometers, and should be taken into account when dealing with the coarsening phenomenon, but we leave it to another paper's focus and intentionally do not address it in this paper.

3. Calculation of capillary force

Consider a pair of identical Pt/C particles, as shown in Fig. 2, whose surfaces are hydrophilic. Inside the space between the Pt/C particles, capillary condensation can occur at the equilibrium vapor pressure p below the saturation vapor pressure p_0 [13]. The relation between $p$and p_0 can be described by the Kelvin equation,

$$\ln\frac{p}{p_0} = \frac{2D\gamma_{LV}V_m}{kT} \tag{1}$$

where V_m is the molar volume of water, γ_{LV} is the surface tension as a function of temperature given in Table 1, k is the Boltzmann constant and T is the absolute temperature, D denotes the mean curvature defined as

$$2D = \left(\frac{1}{r_1} + \frac{1}{r_2}\right) \tag{2}$$

where r_1 and r_2 are the two principle radii of the water-vapor interface. The radius sign is positive if the surface is convex to the liquid and negative if concave to the liquid.

Substituting Eq. (2) into Eq. (1) yields

$$kTV_m^{-1}\gamma_{LV}^{-1}\ln\frac{p}{p_0} = \left(\frac{1}{r_1} + \frac{1}{r_2}\right) \tag{3}$$

Consider a pair of identical solid Pt/C spheres, as shown in

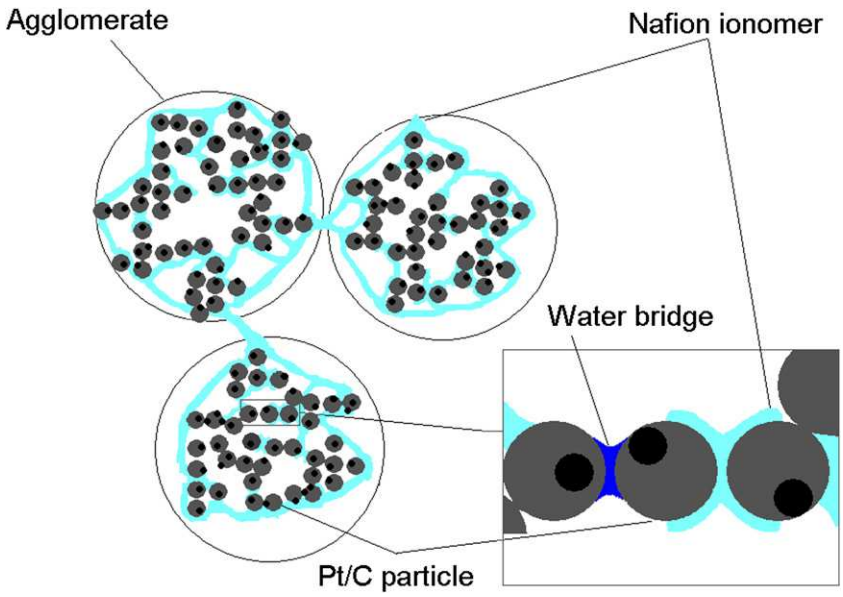

Fig. 1 – A water-bridge in the microstructures of a catalyst layer.

Fig. 2, with a water-bridge in between the two spheres. The radius of the two identical solid spheres is expressed by R and the distance between them is denoted by H. The radii of the liquid bridge are r_1 in plane and r_2 through plane. The water contact angle is θ and the apparent contact angle is α. Using the geometry relationship called toroidal approximation [16,17], we can have

$$r_1 = \frac{H/2 + R(1-\cos\alpha)}{\cos(\alpha+\theta)} \tag{4}$$

$$r_2 = R\sin\alpha - [1-\sin(\alpha+\theta)]r_1 \tag{5}$$

Substituting Eqs. (4) and (5) into Eq. (3) yields

$$kTV_m^{-1}\gamma_{LV}^{-1}\ln\frac{p}{p_0} = \frac{1}{R\sin\alpha - [1-\sin(\alpha+\theta)]\left[\frac{H/2+R(1-\cos\alpha)}{\cos(\alpha+\theta)}\right] - \frac{\cos(\alpha+\theta)}{H/2+R(1-\cos\alpha)}} \tag{6}$$

Eq. (6) says that α is a function of T and p/p_0 when water contact angle and geometry parameters are given,

$$\alpha = \alpha\left(T, \frac{p}{p_0}\right) \tag{7}$$

Eq. (6) is a transcendental equation and thus needs to be solved by numerical methods (such as the Newton–Raphson scheme) to get an approximate solution.

After substituting Eq. (7) into Eqs. (4) and (5), one can see that r_1 and r_2 can be expressed by T and p/p_0,

$$r_1 = r_1\left(T, \frac{p}{p_0}\right) \tag{8}$$

$$r_2 = r_2\left(T, \frac{p}{p_0}\right) \tag{9}$$

Eqs. (7)–(9) says that the water-bridge's geometry is completely determined by T and p/p_0.

Given the water-bridge's geometry, we can calculate the capillary force F, a force that the water-bridge exerts on the solid Pt/C spheres. There are two methods available [18,19] for

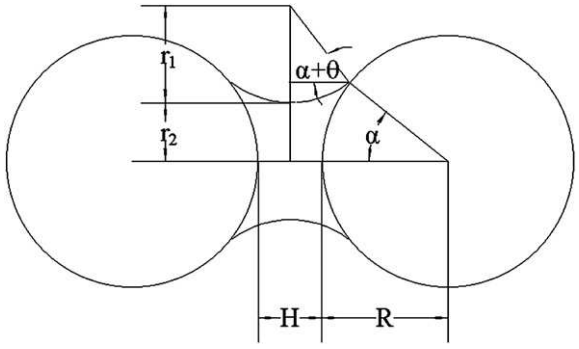

Fig. 2 – Geometrical description of the water-bridge formed between two spheres.

Table 1 – Water surface tension under different temperatures.

Temperature	Surface tension in contact with air 10^{-2} Nm^{-1}
0	7.56
10	7.42
20	7.28
30	7.12
40	6.96
50	6.79
60	6.62
70	6.44
80	6.26
90	6.08
100	5.89

calculating the force. In this paper, we use the gorge method provided by [19] which is believed to have a better estimate of the total force,

$$F = -\pi r_2^2 \Delta p + 2\pi r_2 \gamma_{LV} \tag{10}$$

where the capillary pressure Δp is given by the Young–Laplace equation

$$\Delta p = \gamma_{LV}\left(\frac{1}{r_1} + \frac{1}{r_2}\right) \tag{11}$$

Substituting Eq. (11) to Eq. (3), yields

$$\Delta p = kTV_m^{-1}\ln\frac{p}{p_0} \tag{12}$$

Furthermore, substituting Eqs. (8), (9) and (12) to Eq. (10), we can relate the capillary force F, with T and p/p_0, as shown below,

$$F = -\pi\left[r_2\left(T, \frac{p}{p_0}\right)\right]^2 kTV_m^{-1}\ln\frac{p}{p_0} + 2\pi r_2\left(T, \frac{p}{p_0}\right)\gamma_{LV} \tag{13}$$

Replacing p/p_0 with the relative humidity value (RH) according to its definition, Eq. (13) can be rewritten as,

$$F = -\pi[r_2(T, RH)]^2 kTV_m^{-1}\ln RH + 2\pi r_2(T, RH)\gamma_{LV} \tag{14}$$

4. Parametric studies

The above equations show that the capillary force is a complex function of the variables including the relative humidity, the temperature, the water contact angle, the size of Pt/C particles and the distance between them. We purposely selected a group of values for the variables and calculated the capillary force associated with the group of values. The values for temperature are selected as 20 °C, 50 °C, and 80 °C adopted in our previous work [9]. The values for the radius of Pt/C particles are 10 nm, 15 nm and 20 nm. It was observed that the surface of the catalyst layer is hydrophobic and will become hydrophilic due to contaminations [20]. However, the water contact angle on the surface of Pt/C particles in catalyst layers is experimentally unavailable. Since platinum particle is hydrophilic, the wetability of the surface may vary from the sites with Pt particles, the sites without Pt, and different carbon supports such as, Vulcan, Ketjen-Black and graphitized Ketjen-Black etc. Different function groups on the carbon support resulted from operations also change the wetability of the surface of Pt/C particles. The wetability also depends on the Pt loading, the distribution of Pt particles and possible contaminations. Thus we use the water contact angle values as low as 20°, 40° and 60° for performing the parametric study and investigate how the values influence the capillary condensation.

As to the distances between Pt/C particles, references [21,22] conclude that in the microstructures of the catalyst layers the pore size between carbon agglomerates ranges around dozens of nanometers and the pore size between Pt/C particles inside the agglomerates ranges around several nanometers. According to the solving equations in Section 3, the capillary condensation starts from smaller hydrophilic pores and expands to larger hydrophilic pores with the accumulation of liquid water. Therefore we select the distances as 1 nm and 2 nm that represent those domains with small pores in the microstructures where the condensation may occur first.

4.1. *Relative humidity and temperature*

The dependence of the capillary force upon relative humidity and temperature is shown in Fig. 3. There are three curves showing the relation between capillary force and relative humidity. The yellow, pink and blue curves are associated with temperature 20 °C, 50 °C and 80 °C, respectively. The radius of the pair of Pt/C particles is 20 nm and their water contact angle is 20°. The distance between the two particles is taken as $H = 1$ nm. It can be seen from Fig. 3 that the capillary force does not exist when RH is lower than a certain value, implying that no water-bridge is formed. It can also be seen that the capillary force becomes larger when RH value is getting higher, indicating that the size of water-bridge gets larger when RH value becomes higher. In addition, the figure shows that it takes higher RH value to form a water-bridge at high temperature than at low temperature. This is mainly due to the decrease of water surface tension when temperature goes up.

4.2. *Water contact angle and geometry parameter*

Fig. 4 lists the three curves about the relation between capillary force and relative humility RH at different water contact

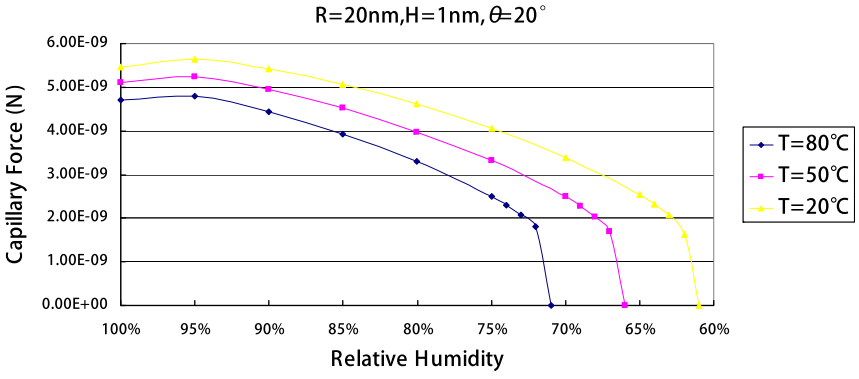

Fig. 3 – Capillary forces under different relative humidity when the temperature is 80 °C, 50 °C and 20 °C.

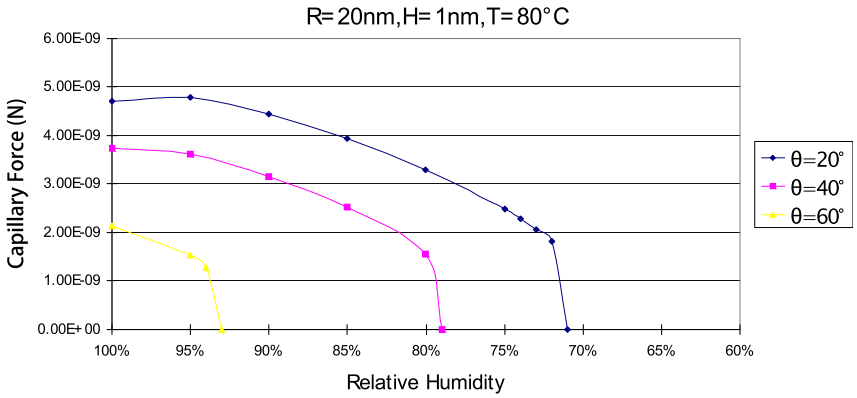

Fig. 4 – Capillary forces under different relative humidity when water contact angle is 20°, 40° and 60°.

angles (20°, 40° and 60°). As can be seen from Fig. 4, the curve associated with a high value of water contact angle is below that associated with a low water-contact angle, which suggests that a large water contact angle leads to a small water-bridge and thus a small capillary force. Here we assume the radius of the pair of Pt/C particles is $R = 20$ nm and temperature $T = 80$ °C.

Fig. 5 shows the relation between capillary force and RH with respect to three different size of Pt/C particles ($R = 10$ nm, $R = 15$ nm and 20 nm). The three curves indicate that the capillary force gets weaker when the radius of Pt/C particle gets smaller. The curves also indicate that it is more difficult to form a water-bridge between a pair of smaller particles than a pair of larger ones. The larger the radius of the Pt/C particles is, the larger the capillary force. But the rate of the increase of capillary force is not as high as the rate of increase of the surface area of Pt/C particles, which can be seen from Fig. 5. The surface area of the Pt/C particle with radius 20 nm is 4 times as large as that of the Pt/C particle with radius 10 nm, but the capillary force associated with the 20 nm Pt/C particle is only two times as large as that of the Pt/C particle with 10 nm radius. The reason for comparing the rate of the increase of capillary force induced by an increase of Pt/C particle's radius with the rate of the Pt/C particle's surface area is for figuring out how the Pt/C particle's size could affect the adhesion strength at the interface between the Pt/C particle's surface and Nafion ionomer. If we can assume that the adhesion strength at the interface between the Pt/C particle's surface and Nafion ionomer is proportional to the surface area of the Pt/C particle, we can conclude that the larger the size of the Pt/C particles is, the less likely that delamination and cracks at the interface happen.

In Fig. 6, we compared the effect of the distance between the pair of Pt/C particles upon capillary force. The pink curve corresponds to $H = 2$ nm and the blue curve to $H = 1$ nm. The two curves show clearly that it takes a higher value of RH to form a water-bridge when the distance of the pair of Pt/C particles is longer than the RH value needed to form a water-bridge when the distance is shorter. Given the same RH value, the capillary force associated with a longer distance H is smaller than with a shorter distance H.

5. Mechanical properties of Nafion, Pt/C particles and their interfaces

In catalyst layers Pt/C particles and Nafion form random porous structure in nano-scale, so it is difficult to determine the material parameters at this stage. More experiments or molecular simulations need to be done to determine their characteristics. In this section, we use bulk material models to describe the stress-versus-strain relationship of Nafion and Pt/C particles and also the mechanical properties of the interface between Nafion and Pt/C particles.

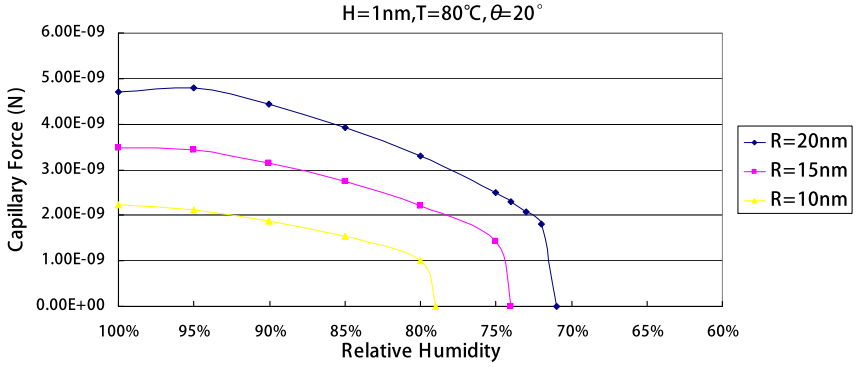

Fig. 5 – Capillary forces under different relative humidity when the sphere radii are 20 nm, 15 nm and 10 nm.

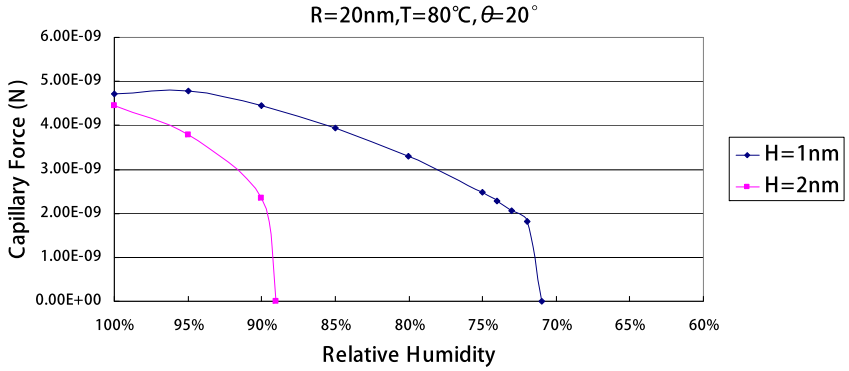

Fig. 6 – Capillary forces under different relative humidity when the gap distance are 1 nm and 2 nm.

5.1. *Mechanical properties of Nafion and Pt/C particles*

Based on experiments data in references [23–27], a piecewise linear isotropic elastic-plastic-failure model, as shown in Fig. 7, was used to describe the mechanical behavior of Nafion. In this model, the Young's modulus E_0, the plastic modulusE_1, the yield stress σ_p and the failure stress σ_s vary with relative humidity and temperature. For example, The Young's modulus E_0 is illustrated in Fig. 8 and other parameters can be found in reference [9].

The Mises yield criterion is adopted as the yield criterion of the Nafion in catalyst layers. It assumes that yield occurs when the Mises yield function approaches zero. The Mises yield function is given as

$$f(\boldsymbol{\sigma}) = \sqrt{\frac{3}{2}\mathbf{S}\mathbf{S}} - \sigma_p \tag{15}$$

where $\boldsymbol{\sigma}$ is the stress tensor, $\boldsymbol{\sigma}_p$ is the yield stress of the material, and $\mathbf{S}$ is the deviatoric stress. According to the Mises yield criterion, yield occurs when $f(\boldsymbol{\sigma}) = 0$. For $f(\boldsymbol{\sigma}) < 0$, the Nafion exhibits an elastic behavior.

Reference [28] indicates that the Nafion is much softer than the Pt/C particles, meaning that the Pt/C particle can be considered as an elastic material without any plastic deformation in it. The Young's modulus of the Pt/C particle is 4.8 GPa according to reference [28].

5.2. *The mechanical model of the interface between Nafion and Pt/C particles*

In order to calculate stress and strain at the interface between Nafion thin-film and Pt/C particles, the technique called the cohesive zone model (CZM) was used. The CZM adopts softening relationship between traction and separation, which in turn define a critical fracture energy that is the indicator of breaking-apart at the interface surfaces. A special set of interface elements is used to represent the interface surfaces between Nafion and Pt/C particles, and the CZM is used to represent the interface constitutive behavior.

The CZM is a constitutive relation between the traction acting on the interface and the corresponding interfacial separation $\boldsymbol{\delta}$. For interface elements, the interfacial separation is defined as displacement jump across the interface, which means the difference of the displacements of the adjacent interface surfaces. Here we should mention that the definition of the separation is based on local element coordinate system. The separation along local normal direction is denoted as δ_n

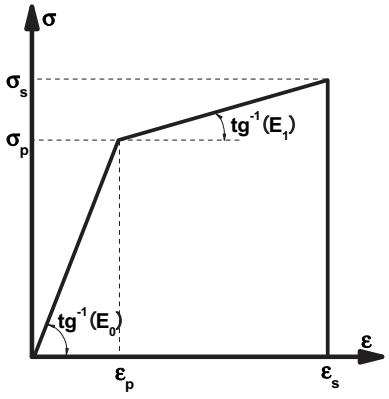

Fig. 7 – The piecewise linear constitutive relationship of Nafion adopted in the model.

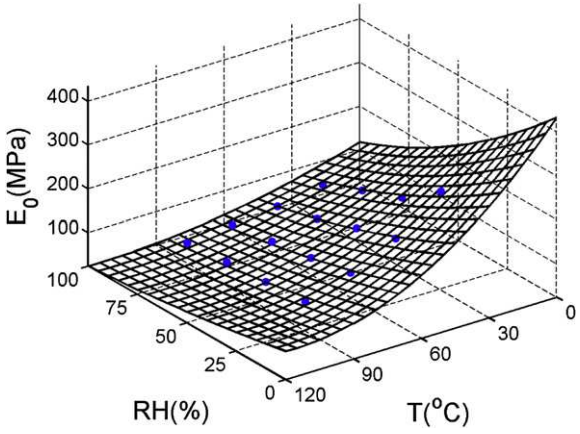

Fig. 8 – Young's modulus as functions of temperature and relative humidity.

and separation along local tangent direction is denoted as δ_t. An exponential form of the CZM, originally proposed by Xu and Needleman, uses a surface potential,

$$\Phi(\boldsymbol{\delta}) = e\sigma_{\max}\overline{\delta}_n\left[1-\left(1+\frac{\delta_n}{\overline{\delta}_n}\right)\exp\left(-\frac{\delta_n}{\overline{\delta}_n}\right)\exp\left(-\frac{\delta_t^2}{\overline{\delta}_t^2}\right)\right] \tag{16}$$

where $\Phi(\boldsymbol{\delta})$ is the surface potential, e is Euler's number (2.7182…), $\sigma_{\max}$ is the maximum normal traction at the interface. δ_n is the normal separation across the interface, δ_t is the shear separation along the interface, $\overline{\delta}_n$ is the normal separation where the maximum normal traction is attained with $\delta_t = 0$, and $\overline{\delta}_t$ is the shear separation where the maximum shear traction is attained at $\delta_t = \overline{\delta}_t/\sqrt{2}$. So the traction (on both the normal direction and the shear direction) can be defined as

$$T_n = \frac{\partial\Phi}{\partial\delta_n} \text{ and } T_t = \frac{\partial\Phi}{\partial\delta_t}. \tag{17}$$

From Eqs. (16) and (17), the normal traction of the interface is

$$T_n = e\sigma_{\max}\frac{\delta_n}{\overline{\delta}_n}\exp\left(-\frac{\delta_n}{\overline{\delta}_n}\right)\exp\left(-\frac{\delta_t^2}{\overline{\delta}_t^2}\right) \tag{18}$$

and the shear traction is

$$T_t = 2e\sigma_{\max}\frac{\overline{\delta}_n\delta_t}{\overline{\delta}_t^2}\left(1+\frac{\delta_n}{\overline{\delta}_n}\right)\exp\left(-\frac{\delta_n}{\overline{\delta}_n}\right)\exp\left(-\frac{\delta_t^2}{\overline{\delta}_t^2}\right) \tag{19}$$

From the publication on the interface of polymer (such as epoxy or PTFE) and the carbon nanotube [29], the maximum normal traction $\sigma_{\max}$ is close to $E_0/10$, where E_0 is the Young's modulus of Nafion. The normal characteristic separation $\overline{\delta}_n$ is taken to be the same as the shear characteristic separation $\overline{\delta}_t$ [30]. The maximum shear stress is close to $\sigma_p/\sqrt{3}$, where σ_p is the yield stress of Nafion.

6. Stress induced by periodic capillary force

In this section, we use the finite element method to calculate the stress and strain inside the Nafion thin-film, which connects with one of the pair of Pt/C particles. Between the pair of the Pt/C particles there is a water-bridge exerting a capillary force on the Pt/C particles. The objective is to find whether or how it affects the failure of Nafion domain and the interface delamination.

First of all, we should mention that this numerical example is simulated to analyze qualitatively the mechanism of the microstructure evolution in the catalyst layers. We cannot give the results of quantitative analysis at this stage because the actual conditions in catalyst layers are highly random and complicated and the geometry and material parameters are difficult to be determined.

It is assumed that two Pt/C particles are linked by Nafion thin-film, which partly covers on the Pt/C particle surface. The model details are listed in Table 2. Utilizing the axisymmetric microstructure, we need only to mesh a quarter of the whole geometry, as shown in Fig. 9. The left side of the left particle is fixed and the capillary force is applied on the exposed outside surface of the right side particle. The dynamic load in the form of dynamic relative humidity is shown in Fig. 10 ranging from 35% to 95%, which leads to the fluctuation of capillary force. The capillary force was calculated using the equations in Section 3. Here the thermal and swelling expansion of Nafion is not considered. CZM elements are defined on the interface between Nafion thin-film and the two Pt/C particles.

Table 2 – Geometry and operational parameters in stress simulation.

Radius of each particle (nm)	20
Distance between two particles connected by Nafion film (nm)	2
Thickness of the Nafion film (nm)	5
Distance between two particles between which water-bridge generates (nm)	2
Constant temperature in simulation (°C)	80
Relative humidity (%)	Fig. 10
Water contact angle on the surface of Pt/C particle (degree)	40

The FEM software package ANSYS 12 was used for the simulations. The results of the simulations show that the mechanical status in this microstructure tends to be steady after first several cycles of relative humidity. The contours of von Mises stress in the Nafion thin-film under different load steps are illustrated in Fig. 11(a) and (b). The figures show that the von Mises stress inside Nafion reaches as high as 3.61 MPa at relative humidity 95%. This stress level exceeds the yield stress of Nafion $\sigma_p = 2.98$ MPa, leading to plastic deformation. The results also indicate that the von Mises stress fluctuates under different load steps. Although the maximum of stress does not exceed the breaking-apart stress of Nafion σ_s, cracks could happen in the form of material fatigue after a number of dynamic load cycles. This will eventually cause the movement of Pt/C particles, furthering Pt/C-particle-agglomeration. Finally, mechanical change in the microstructure leads to the degradation of catalyst layers.

Fig. 12(a) and (b) show the normal stress contours on the interface of the Nafion thin-film and the two Pt/C particles under different load steps after first several cycles of relative humidity. The figures show that the maximum value of the normal stress on the interface achieves 13.8 MPa at relative humidity of 95%, which is very close to the Nafion material strength limit $\sigma_{\max}$ 14.8 MPa. At the load step of relative humidity RH = 35%, the maximum value of the normal stress decreases to 0.743 MPa and the level of the normal stress is generally much lower than that when RH = 95%. Although

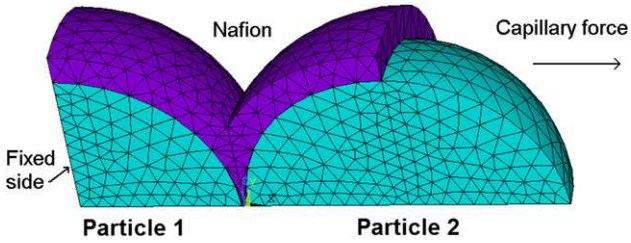

Fig. 9 – A quarter of 3-D microstructure contains Pt/C particles and Nafion.

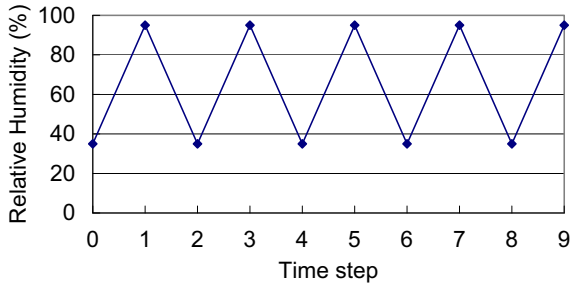

Fig. 10 – Dynamic load cycles of relative humidity.

there is no normal stress exceeding the maximum normal traction σ_{max}, it is reasonable to anticipate that mechanical fatigue could happen under such a high stress level after a certain number of load cycles. All the results above show that the capillary force is in the same order of magnitude as the force that causes the rupture of the Nafion thin-film and/or delamination between the Nafion thin-film and Pt/C particles.

Some idealizations in the way we model it perhaps underestimate the stress and strain. We didn't consider the effect of carbon's or Nafion's deformation on the capillary force. The real capillary force should be larger than those calculated in these simulations. When the gap between two spheres gets narrower under external loads, the capillary force will become larger according to the results of parametric study obtained in Section 4. Furthermore, when the rupture of the Nafion thin-film and/or delamination along interfaces occur, the Pt/C particles will not be fixed anymore and free to move. The water-bridge between the two free solid particles will adjust its shape and tend to drag the solid phases together to keep total surface energy minimum [31], which is what we suggest as an explanation of the phenomena of agglomerate coarsening in the catalyst layers.

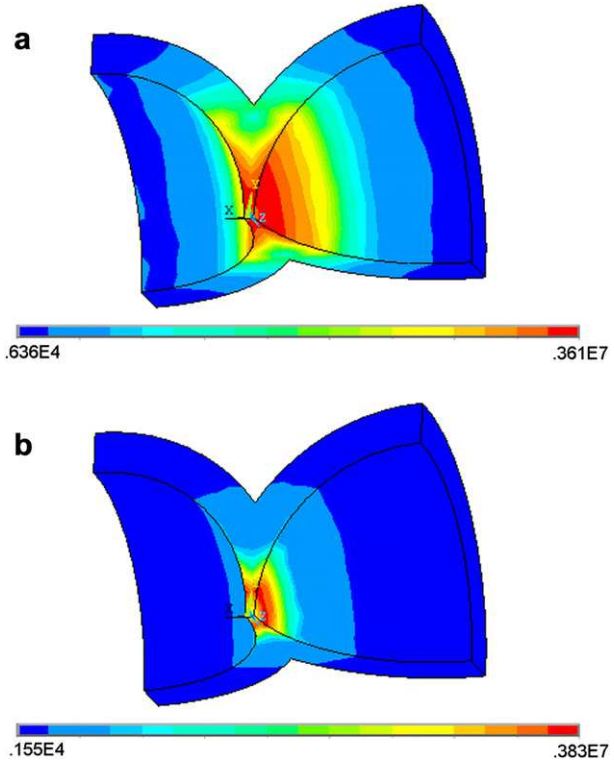

Fig. 11 – Contours of von Mises stress in Nafion domain after first several load cycles (a) Von Mises stress in Nafion when RH = 95% (b) Von Mises stress in Nafion when RH = 35%.

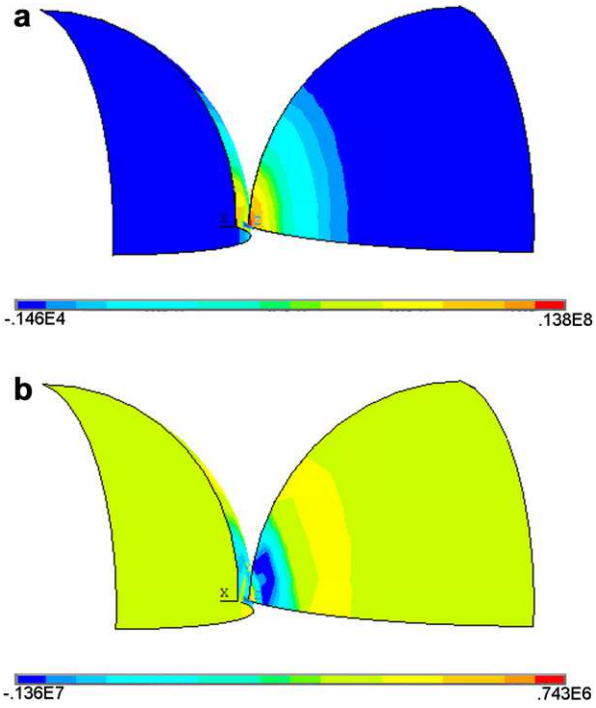

Fig. 12 – Contours of normal stress on the interfaces after first several load cycles (a) Normal stress on the interfaces when RH = 95% (b) Normal stress on the interfaces when RH = 35%.

7. Concluding remarks

This paper investigates the capillary condensation and its effect on the microstructure changes of the catalyst layers of PEM fuel cells. The hypothesis is proposed for explaining the effect of dynamic operating conditions on microstructure changes. The relation between capillary force and the factors such as temperature and relative humidity is derived based the Kelvin equation, and the effect of water contact angle and geometry parameters of the Pt/C particles on the capillary force is analyzed. Furthermore the finite element method is used to model a specific microstructure with Pt/C particles and Nafion thin-film. Because the microstructures in catalyst layers are random and heterogeneous, also the parameters of the materials are difficult to determine, the simulations only give the qualitative analysis on the evolutional mechanism. The numerical results show that the von Mises stress level can as high as the breaking stress level, meaning that the failure of

Nafion thin-film and the delamination along the interfaces could happen. This supports the hypothesis that capillary condensation can cause the movement of Pt/C particles towards to each other.

Acknowledgments

Liang Ma thanks the China Scholarship Council and the National Research Council Canada (NRC) for the financial support through the NRC-MOE Research and Post-doctoral Fellowship Program, which allows Liang Ma to spend his one-year research-stay at NRC.

REFERENCES

[1] Wilkinson DP, St-Pierre J. Durability. In: Vielstich W, Gasteiger HA, Lamm A, editors. Handbook of fuel cells-fundamental, technology and applications. Chichester: John Wiley & Sons; 2003. p. 612–26.
[2] Knights SD, Colbow KM, St-Pierre J, Wilkinson DP. Aging mechanisms and lifetime, PEFC and DMFC. J Power Sources 2004;127:127–34.
[3] Xie J, Wood DL, More KL, Atanassov P, Borup RL. Microstructural changes of membrane electrode assemblies during PEFC durability testing at high humidity conditions. J Electrochem Soc 2005;152:A1011–20.
[4] Xie J, Wood DL, Wayne DM, Zawodzinski TA, Atanassov P, Borup RL. Durability of PEFCs at high humidity conditions. J Electrochem Soc 2005;152:A104–13.
[5] Kundu S, Fowler MW, Simon LC, Grot S. Morphological features (defects) in fuel cell membrane electrode assemblies. J Power Sources 2006;157:650–6.
[6] McDonald RC, Mittelsteadt CK, Thompson EL. Effects of deep temperature cycling on Nafion® 112 membranes and membrane electrode assemblies. Fuel Cells 2004;4:208–13.
[7] Kusoglu A, Karlsson AM, Santare MH, Cleghorn S, Johnson WB. Mechanical response of fuel cell membranes subjected to a hygro-thermal cycle. J Power Sources 2006;161:987–96.
[8] Tang Y, Santare MH, Karlsson AM, Cleghorn S, Johnson WB. Stresses in proton exchange membranes due to hydro-thermal loading. J Fuel Cell Sci Technol 2006;3:119–24.
[9] Rong F, Huang C, Liu ZS, Song DT, Wang QP. Microstructure changes in the catalyst layers of PEM fuel cells induced by load cycling. Part I. Mechanical model. J Power Sources 2008; 175:699–711.
[10] Rong F, Huang C, Liu ZS, Song DT, Wang QP. Microstructure changes in the catalyst layers of PEM fuel cells induced by load cycling. Part II. Simulation and understanding. J Power Sources 2008;175:712–23.
[11] Rowlinson JS, Widom B. Molecular theory of capillarity. Oxford: Oxford University Press; 1989.
[12] Dobbs HT, Yeomans JM. Capillary condensation and prewetting between spheres. J Phys. Condens Matter 1992;4: 10133–8.
[13] Nowak D, Christenson HK. Capillary condensation of water between mica surfaces above and below zero-effect of surface ions. Langmuir 2009;25:9908–12.
[14] Zienkiewicz OC, Taylor RL. The finite element method. 4th ed. New York: McGraw-Hill; 1988.
[15] Mu D, Liu ZS, Huang C, Djilali N. Determination of the effective diffusion coefficient in porous media including Knudsen effects. Microfluid Nanofluid 2008;4:257–60.
[16] Pepin X, Rossetti D, Simons SJR. Modeling pendular liquid bridges with a reducing solid-liquid interface. J Colloid Interface Sci 2000;232:298–302.
[17] Mu F, Su X. Analysis of liquid bridge between spherical particles. China Particuology 2007;5:420–4.
[18] Iverson SM, Litster JD, Hapgood K, Ennis BJ. Nucleation, growth and breakage phenomena in agitated wet granulation processes: a review. Powder Technol 2001;117: 3–39.
[19] Lian G, Thornton C, Adams MJ. A theoretical study of the liquid bridge forces between two rigid spherical bodies. J Colloid Interface Sci 1993;161:138–47.
[20] Yu HM, Ziegler C, Oszcipok M, Zobel M, Hebling C. Hydrophilicity and hydrophobicity study of catalyst layers in proton exchange membrane fuel cells. Electrochim Acta 2006;51:1199–207.
[21] Mizuhata H, Nakao SI, Yamaguchi T. Morphological control of PEMFC electrode by graft polymerization of polymer electrolyte onto platinum-supported carbon black. J Power Sources 2004;138:25–30.
[22] Xie Z, Navession T, Shi K, Chow R, Wang Q, Song D, et al. Functionally graded cathode catalyst layers for polymer electrolyte fuel cells. J Electrochem Soc 2005;152:1171–9.
[23] Satterfield MB, Majsztrik PW, Ota H, Benziger JB, Bocarsly AB. Mechanical properties of Nafion and titania/Nafion composite membranes for polymer electrolyte membrane fuel cells. J Polym Sci. Part B Polym Phys 2006;44:2327–45.
[24] Chen X, Hui S. Ratcheting behavior of PTFE under cyclic compression. Polym Test 2005;24:829–33.
[25] Kundu S, Simon LC, Fowler M, Grot S. Mechanical properties of Nafion™ electrolyte membranes under hydrated conditions. Polymer 2005;46:11707–15.
[26] Morris DR, Sun X. Water-sorption and transport properties of Nafion 117 H. J Appl Polym Sci 1993;50:1445–52.
[27] Gebel G, Aldebert P, Pineri M. Swelling study of perfluorosulphonated ionomer membranes. Polymer 1993; 34:333–9.
[28] Matweb. Available from, http://www.matweb.com.
[29] Liljedahl CDM, Crocombe AD, Wahab MA, Ashcroft IA. Damage modelling of adhesively bonded joints. Int J Fract 2006;141:147–61.
[30] Xu XP, Needleman A. Numerical simulations of fast crack growth in brittle solids. J Mech Phys Solids 1994;42:1397–434.
[31] Zheng J, Streator JL. A generalized formulation for the contact between elastic spheres: applicability to both wet and dry conditions. J Tribol 2007;129:274–82.